Correlation of Structure, Tunable Colors, and Lifetimes of (Sr, Ca, Ba)Al$_2$O$_4$:Eu^{2+}, Dy^{3+} Phosphors

Qidi Xie [1], Bowen Li [1,2], Xin He [1,*], Mei Zhang [1,*], Yan Chen [1] and Qingguang Zeng [1]

[1] School of Applied Physics and Materials, Wuyi University, Jiangmen 529020, China; qidixie@163.com (Q.X.); libowenliboyuan@126.com (B.L.); ychen08@163.com (Y.C.); zengqg1979@126.com (Q.Z.)

[2] School of Materials Science and Engineering, Harbin Institute of Technology, Harbin 150001, China

* Correspondence: hexin@mail.wyu.edu.cn (X.H.); zmjenny@163.com (M.Z.)

Abstract: (Sr, Ca, Ba)Al$_2$O$_4$:Eu^{2+}, Dy^{3+} phosphors were prepared via a high temperature solid-state reaction method. The correlation of phase structure, optical properties and lifetimes of the phosphors are investigated in this work. For the (Sr, Ca)Al$_2$O$_4$:Eu^{2+}, Dy^{3+} phosphors, the different phase formation from monoclinic SrAl$_2$O$_4$ phase to hexagonal SrAl$_2$O$_4$ phase to monoclinic CaAl$_2$O$_4$ phase was observed when the Ca content increased. The emission color of SrAl$_2$O$_4$:Eu^{2+}, Dy^{3+} phosphors varied from green to blue. For the (Sr, Ba)Al$_2$O$_4$:Eu^{2+}, Dy^{3+} phosphors, different phase formation from the monoclinic SrAl$_2$O$_4$ phase to the hexagonal BaAl$_2$O$_4$ phase was observed, along with a shift of emission wavelength from 520 nm to 500 nm. More interestingly, the decay time of SrAl$_2$O$_4$:Eu^{2+}, Dy^{3+} changed due to the different phase formations. Lifetime can be dramatically shortened by the substitution of Sr^{2+} with Ba^{2+} cations, resulting in improving the performance of the alternating current light emitting diode (AC-LED). Finally, intense LEDs are successfully obtained by combining these phosphors with Ga(In)N near UV chips.

Keywords: phosphors; solid solution; average lifetime; AC-LEDs; photoluminescence

1. Introduction

AC-LED is a new type of device that can be directly driven by the alternating current of city power. It has experienced rapid development and is widely applied in indoor and outdoor lighting due to its long life, low price, high efficiency, etc. [1–4].However, the vital defect of the AC-LED is the flickering effect, with a time gap of 5–20 ms [4–6], resulting in visual fatigue and health hazards. There have been several solutions to reduce flashing in AC-LED, such as using a converter-free AC-LED driver, increasing drive frequency etc. However, these solutions suffer from low power efficiency or large size. Fortunately, the use of long afterglow phosphors is considered to be a promising method to compensate for the time gap and reduce the flickering effect. Long afterglow phosphors, such as SrSi$_2$O$_2$N$_2$:Eu^{2+}, Mn^{2+} [2], SrAl$_2$O$_4$:Eu^{2+}, Ce^{3+}, Li$^+$ [5], and SrAl$_2$O$_4$:Eu^{2+}, and RE^{3+} (RE = Y, Dy) have been studied and applied to AC-LEDs [4,7].

SrAl$_2$O$_4$:Eu^{2+} is one of green phosphors for UVLEDs. When it is co-doped with RE^{3+} (RE = Dy, Y, Nd and Ho), SrAl$_2$O$_4$:Eu^{2+}, Re^{3+} can store electrons to achieve long and persistent luminescence. However, the afterglow time of SrAl$_2$O4:Eu^{2+}, Dy^{3+} is too long to fulfill the requirement of AC-LED. In our previous research, we shortened the average lifetime of SrAl$_2$O$_4$:Eu^{2+}, Dy^{3+} phosphors from 845.86 ms to 428.83 ms by changing the amount of SrCl$_2$ flux. Moreover, MAl$_2$O$_4$:Eu^{2+}, Dy^{3+} (M = Ca^{2+}, Sr^{2+}, Ba^{2+}) phosphors with different cations also have different defect levels and afterglow times [7–13]. Therefore, the substitution of Sr^{2+} by Ca^{2+} or Ba^{2+} ions in SrAl$_2$O$_4$:Eu^{2+}, Dy^{3+} phosphors is expected to tune the afterglow time. Furthermore, the emission and excitation spectra of Eu^{2+} ions can also be modified by the different radius of Ca^{2+}, Sr^{2+} and Ba^{2+} ions and crystal structures [13–16].

This paper aims to improve the emission color and the average lifetime of $SrAl_2O_4:Eu^{2+}$, Dy^{3+} phosphors by partially substituting Sr^{2+} with Ca^{2+} or Ba^{2+} ions. The effect and correlation of Ca^{2+} or Ba^{2+} ions substitution on the obtained phases, optical properties, and decay times of $SrAl_2O_4:Eu^{2+}$, Dy^{3+} phosphors are systematically investigated. The electroluminescent properties of the as-fabricated LEDs based on UV-chips and $MAl_2O_4:Eu^{2+}$, Dy^{3+} (M = Ca^{2+}, Sr^{2+}, Ba^{2+}) phosphors are also investigated.

2. Experimental Procedure

$Sr_{0.90-x}Ca_xAl_2O_4:0.05Eu^{2+}$, $0.05Dy^{3+}$ and $Sr_{0.90-y}Ba_yAl_2O_4:0.05Eu^{2+}$, $0.05Dy^{3+}$ samples (x or y = 0.00, 0.15, 0.30, 0.45, 0.60, 0.75, 0.90) were prepared by a high temperature solid-state reaction method. The raw materials $CaCO_3$ (99.99%), $SrCO_3$ (99.99%), $BaCO_3$ (99.99%), Al_2O_3 (99.99%), Eu_2O_3 (99.99%), Dy_2O_3 (99.99%) and H_3BO_3 (99.99%) were weighted stoichiometrically. The original materials were mixed into an agate mortar and placed into a small alumina crucible. Then, the mixtures were put into a tubular furnace and heated to 900 °C for 2 h. Being reground, they were heated to 1400 °C for 4 h under a reductive atmosphere from burning activated carbon. Finally, the samples were cooled to room temperature, resulting in $Sr_{0.9-x}Ca_xAl_2O_4:0.05Eu^{2+}$, $0.05Dy^{3+}$, and $Sr_{0.9-y}Ba_yAl_2O_4:0.05Eu^{2+}$, $0.05Dy^{3+}$ compounds.

The structure of $Sr_{0.90-x}Ca_xAl_2O_4:0.05Eu^{2+}$, $0.05Dy^{3+}$, and $Sr_{0.90-y}Ba_yAl_2O_4:0.05Eu^{2+}$, $0.05Dy^{3+}$ phosphors were explored by X-ray powder diffraction (XRD) using a Diffractometer (X′ Pert PRO, Panalytical, Almelo, Netherlands) with Cu K_α radiation at 40 kV and 20 mA. The data were collected in the 2θ range of 10° to 80°. The photoluminescence (PL) spectra and decay curves were performed by a spectrofluorometer (F-4600, Hitachi, Tokyo, Japan) equipped with a 150W Xe lamp as the light source.

The phosphors were pre-coated on near-UV Ga(In)N chips with 365 and 395 nm emission, respectively. The emission spectra and parameters of the as-fabricated LEDs were measured by the LED spectrophotocolorimeter (PMS 50, Everfine Co., Ltd., Hangzhou, China) with an integrating sphere of 50 cm diameter. The normal forward-bias current was 20 mA. All measurements were conducted at room temperature.

3. Results and Discussion

3.1. X-ray Diffraction Analysis

XRD patterns of $Sr_{0.90-x}Ca_xAl_2O_4:0.05Eu^{2+}$, $0.05Dy^{3+}$ (x = 0.00–0.90) phosphors with various x values are depicted in Figure 1a. The patterns are compared with the JCPDS standard cards of possible phases and marked with different symbols. For $x(Ca^{2+})$ = 0.00, the diffraction peaks are well matched with the monoclinic $SrAl_2O_4$ (MP-$SrAl_2O_4$, JCPDS card No. 74-0794), and minor content of the raw material—Al_2O_3—is observed due to the incomplete reaction, which is explained by our previous work [4]. For $x(Ca^{2+})$ = 0.15, the dominant phase is the hexagonal $SrAl_2O_4$ (HP-$SrAl_2O_4$, JCPDS card No. 31-1336). Thus, the different phase formation from the monoclinic to the hexagonal phase happens in $Sr_{0.90-x}Ca_xAl_2O_4:Eu^{2+}$, Dy^{3+} phosphors when the substitution of Sr^{2+} by Ca^{2+} increases from 0.00 to 0.15. The hexagonal phase remains when $x(Ca^{2+})$ = 0.30. Simultaneously, the MP-$SrAl_2O_4$ disappears and minor content of monoclinic $CaAl_2O_4$ phase emerges. The monoclinic $CaAl_2O_4$ phase (MP-$CaAl_2O_4$, CPDS card No.53-0191) gradually increases with further elevating concentration of Ca^{2+} from 0.45 to 0.75, accompanying with the decrease of HP-$SrAl_2O_4$. For $x(Ca^{2+})$ = 0.90, the dominant phase isMP-$CaAl_2O_4$. In general, as $x(Ca^{2+})$ varies from 0.00 to 0.90, and the obtained phases can be varied as follows: MP-$SrAl_2O_4$ → HP-$SrAl_2O_4$ → MP-Cal_2O_4. Furthermore, it can be concluded that two different phase always coexist due to the cations substitution except for the samples with $x(Ca^{2+})$ = 0.00 and 0.90. The phase change is different with that of other report under different synthesized condition [13].
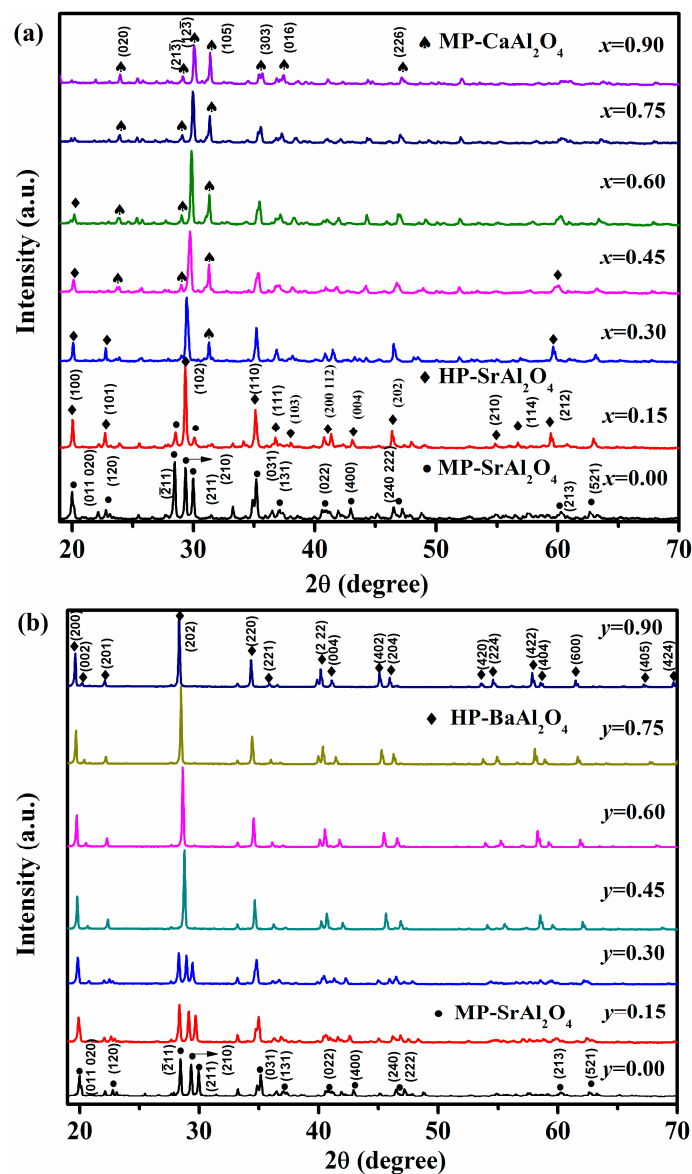
Figure 1. (**a**) X-ray powder diffraction (XRD) patterns of $Sr_{0.90-x}Ca_xAl_2O_4:0.05Eu^{2+}$, $0.05Dy^{3+}$ phosphors with various x (x = 0.00, 0.15, 0.30, 0.45, 0.60, 0.75, 0.90); (**b**) XRD patterns of $Sr_{0.90-y}Ba_yAl_2O_4:0.05Eu^{2+}$, $0.05Dy^{3+}$ phosphors with various y (y = 0.00, 0.15, 0.30, 0.45, 0.60, 0.75, 0.90).

Unlike the substitution of Sr^{2+} by Ca^{2+} in $SrAl_2O_4:Eu^{2+}$, Dy^{3+} phosphors, there is only the variation from MP-$SrAl_2O_4$ to hexagonal $BaAl_2O_4$ phase (HP-$BaAl_2O_4$, JCPDS card No. 17-0306) during the substitution of Sr^{2+} by Ba^{2+}. The coexistence of two phases cannot be observed from the XRD data, as displayed in Figure 2b. Specifically, when $y(Ba^{2+})$ = 0.00–0.30, the crystal structure remains the MP-$SrAl_2O_4$. However, as $y(Ba^{2+})$ = 0.45, the XRD patterns are consistent with the standard HP-$BaAl_2O_4$. It remains unchanged while y varies from 0.45 to 0.90, which stems from the small radius of Sr^{2+} compared to that of Ba^{2+} and the effect of chemical pressure of Ba^{2+} on the crystal structure. Therefore, the $Sr_{0.90-y}Ba_yAl_2O_4:0.05Eu^{2+}$, $0.05Dy^{3+}$ compounds can be regarded as the hexagonal $BaAl_2O_4$ phase replaced by Sr^{2+} ions as $y(Ba^{2+})$ = 0.45–0.90. The different phase formation from MP-$SrAl_2O_4$ to HP-$BaAl_2O_4$ can be obtained when Sr^{2+} is replaced by Ba^{2+} in $SrAl_2O_4:Eu^{2+}$, Dy^{3+} phosphors.
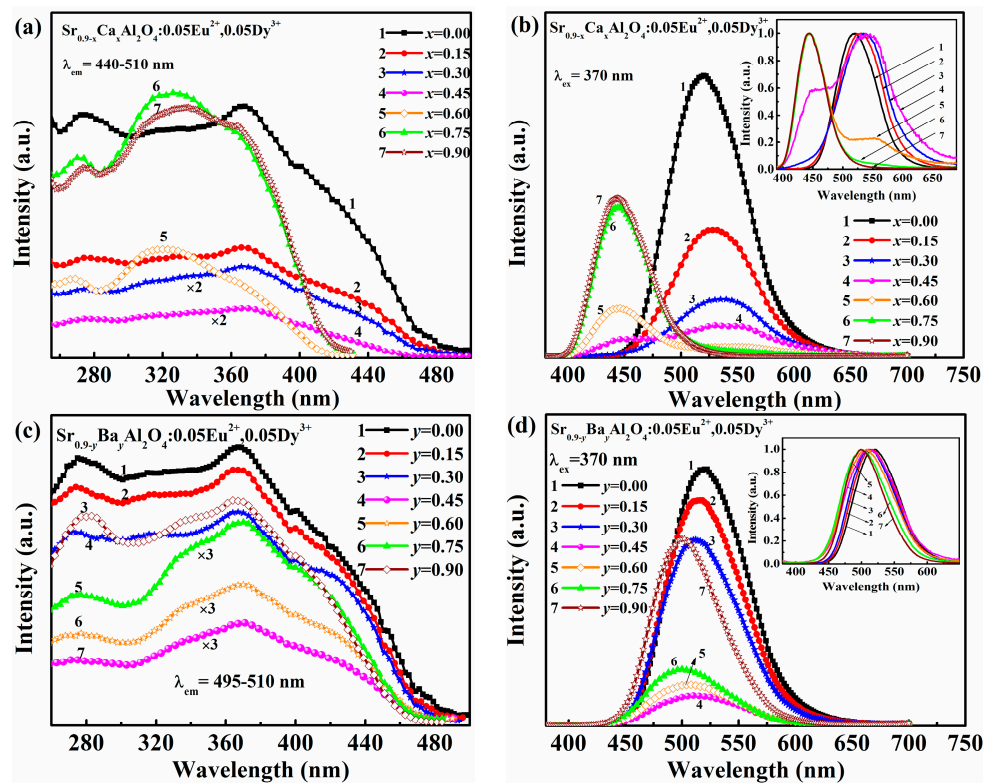
Figure 2. (**a**) Excitation and (**b**) emission spectra of $Sr_{0.90-x}Ca_xAl_2O_4:0.05Eu^{2+}$, $0.05Dy^{3+}$ phosphors with varied *x* values (Inset is the normalized emission spectra of); (**c**) excitation and (**d**) emission spectra of $Sr_{0.90-y}Ba_yAl_2O_4:0.05Eu^{2+}$, $0.05Dy^{3+}$ phosphors with varied *y* values (Inset is the normalized emission spectra).

Another finding is that the peaks of the $Sr_{0.90-x}Ca_xAl_2O_4:0.05Eu^{2+}$, $0.05Dy^{3+}$ shift toward larger 2θ with Ca^{2+} concentration increased (*x* = 0.45–0.90), while the peaks of the $Sr_{0.90-y}Ba_yAl_2O_4:0.05Eu^{2+}$, $0.05Dy^{3+}$ shift to smaller 2θ when Ba^{2+} concentration increased (*y* = 0.00–0.90). Both of these shifts can be explained by the variation of crystal lattice due to the different ionic radius of Ca^{2+}, Sr^{2+}, and Ba^{2+} ions of 0.114 nm, 0.123 nm and 0.134 nm, respectively [13,17]. Therefore, when Sr^{2+} is replaced by Ca^{2+}, the crystal lattice of $SrAl_2O_4$ phase will shrink. On the contrary, it will expand when Sr^{2+} is substituted by Ba^{2+}. Therefore, the difference in the ionic radius leads to the shifts of the diffraction peaks.

3.2. Luminescence Properties of $Sr_{0.09-x}Ca_xAl_2O_4:0.05Eu^{2+}$, $0.05Dy^{3+}$ and $Sr_{0.90-y}Ba_yAl_2O_4:0.05Eu^{2+}$, $0.05Dy^{3+}$ Phosphors

Figure 2 illustrates the emission and excitation spectra of $Sr_{0.90-x}Ca_xAl_2O_4:0.05Eu^{2+}$, $0.05Dy^{3+}$ and $Sr_{0.90-y}Ba_yAl_2O_4:0.05 Eu^{2+}$, $0.05Dy^{3+}$ phosphors with *x*(*y*) ranged from 0.00 to 0.90. The excitation spectra of $Sr_{0.90-x}Ca_xAl_2O_4:0.05Eu^{2+}$, $0.05Dy^{3+}$ phosphors are depicted in Figure 2a with monitoring the emission of Eu^{2+} in the range of 440–510 nm. All samples present broad bands from 250 nm to 450 nm due to $4f^7 \rightarrow 4f^65d^1$ transitions of Eu^{2+} ions [18]. The shape of excitation bands almost remain unchanged while the intensity decreases when *x* value (*x*= 0.00–0.45) increases. However, it should be noted that excitation bands are different from those of *x* < 0.60. The excitation bands of $Sr_{0.90-x}Ca_xAl_2O_4:0.05Eu^{2+}$, $0.05Dy^{3+}$ (*x* = 0.60–0.90) are similar and blue-shift, which is ascribed to the phase variation as discussed in XRD analysis. Figure 2b shows the emission spectra of $Sr_{0.90-x}Ca_xAl_2O_4:0.05Eu^{2+}$, $0.05Dy^{3+}$ phosphors. It can be divided into three sections (*x* = 0–0.30, *x* = 0.45–0.60, *x* = 0.75–0.90). Interestingly, these results are related to the phase transition. First, the luminescence intensity decreases and the emission peak shifts from 520 nm to 538 nm as *x* varied from 0.00 to 0.30. Second, two emission peaks around 450 nm, 540 nm at *x* = 0.45–0.60 are observed due to

the coexistence of heterogeneous mixtures of two structures. Finally, the emission spectrum presents a single peak around 444 nm when x value increased from 0.75 to 0.90, while the dominant phase is monoclinic $CaAl_2O_4$.

The excitation and emission spectra of $Sr_{0.90-y}Ba_yAl_2O_4$:$0.05Eu^{2+}$, $0.05Dy^{3+}$ phosphors are displayed in Figure 2c,d. The excitation spectra show similar outlines with two broad bands around 275 nm, 375 nm and a shoulder around 420 nm. The broad emission bands originate from the typical transitions of $4f^7 \rightarrow 4f^65d^1$ of Eu^{2+} ions, which are affected by the crystal field of host lattice [19]. The emission band shifts to a shorter wavelength from 520 nm to 500 nm as y(Ba^{2+}) increased. It can be explained that the crystal field splitting energy is decreased due to the phase change of the substation of Sr^{2+} by the larger Ba^{2+} ions. However, the luminescence intensity decreases when Ba^{2+} content is 0.00–0.45, while it increases when Ba^{2+} content is 0.60–0.90. These changes match very well with the XRD results mentioned above and can be ascribed to Eu^{2+} emission in different phase.

The CIE chromaticity coordinates calculated from the spectra of $Sr_{0.90-x}Ca_xAl_2O_4$:$0.05Eu^{2+}$, $0.05Dy^{3+}$ and $Sr_{0.9-y}Ba_yAl_2O_4$:$0.05Eu^{2+}$, $0.05Dy^{3+}$ phosphors with varied x (or y) values are presented in Figure 3 and Table 1. These results show that the CIE color coordinates of $SrAl_2O_4$:Eu^{2+}, Dy^{3+} phosphors can be tuned by Ca^{2+} or Sr^{2+} content. For $Sr_{0.90-x}Ca_xAl_2O_4$:$0.05Eu^{2+}$, $0.05Dy^{3+}$ phosphors, the color coordinates can be changed from green (0.2393, 0.5874, point M) to blue (0.1531, 0.0528, point A) area with x increased. In addition, the color coordinates of $Sr_{0.9-y}Ba_yAl_2O_4$:$0.05Eu^{2+}$, $0.05Dy^{3+}$ phosphors have a little shift from green (0.2399, 0.5867, point M) to bluish green (0.1652, 0.4645, point B) area. The above discussion indicates that the emission color of $SrAl_2O_4$:Eu^{2+}, Dy^{3+} can be tuned due to the phase change of the substitution of Sr^{2+} with Ca^{2+} or Ba^{2+} ions. It is an important challenge to tune the color of phosphors for improving the color rendering index of w-LEDs [20–22].
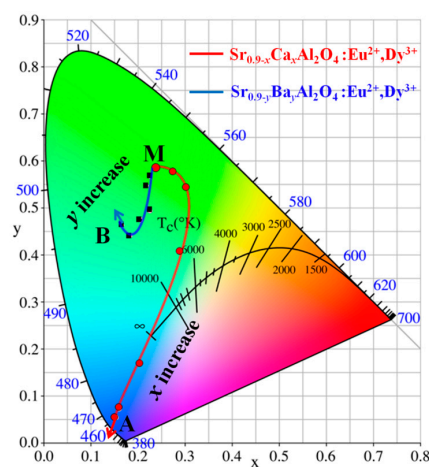

Figure 3. CIE chromaticity diagram of $Sr_{0.90-x}Ca_xAl_2O_4$:$0.05Eu^{2+}$, $0.05Dy^{3+}$ and $Sr_{0.90-y}Ba_yAl_2O_4$:$0.05Eu^{2+}$, $0.05Dy^{3+}$ phosphors with various x (or y) values (x, y= 0.00–0.90).

Table 1. Color coordinates of $Sr_{0.90-x}Ca_xAl_2O_4$:$0.05Eu^{2+}$, $0.05Dy^{3+}$ and $Sr_{0.90-y}Ba_yAl_2O_4$:$0.05Eu^{2+}$, $0.05Dy^{3+}$ phosphors (x, y = 0.00–0.90).

x (or y) Values	$Sr_{0.90-x}Ca_xAl_2O_4$:$0.05Eu^{2+}$, $0.05Dy^{3+}$		$Sr_{0.90-y}Ba_yAl_2O_4$:$0.05Eu^{2+}$, $0.05Dy^{3+}$	
	CIE (x, y)		CIE (x, y)	
	x	y	x	y
0.00	0.2393	0.5874	0.2399	0.5867
0.15	0.2741	0.5754	0.2251	0.5675
0.30	0.3029	0.5456	0.2170	0.5477
0.45	0.2860	0.4086	0.2258	0.4952
0.60	0.2059	0.1712	0.2054	0.4741
0.75	0.1607	0.0729	0.1823	0.4412
0.90	0.1531	0.0528	0.1652	0.4645

3.3. Decay Characteristics

The photoluminescence decay curves of $SrAl_2O_4:Eu^{2+}$, Dy^{3+} phosphors with varied Ca^{2+} and Ba^{2+} content are shown in Figure 4a,b, respectively. The figures reveal the initial luminous intensity is different when Sr^{2+} is replaced by either Ca^{2+} or Ba^{2+} in $SrAl_2O_4:Eu^{2+}$, Dy^{3+}. Among these phosphors, $Sr_{0.90}Al_2O_4:0.05Eu^{2+}$, $0.05Dy^{3+}$ has the highest initial luminous intensity. The initial luminous intensity gradually decreases when the content of $Ca^{2+}(Ba^{2+})$ increased to 0.45. By further increasing the Ca^{2+} or Ba^{2+} concentration, the initial luminous intensity enhances. The variation of initial luminous intensity is consistent with the emission spectra, which can be explained by the change of crystal structure.
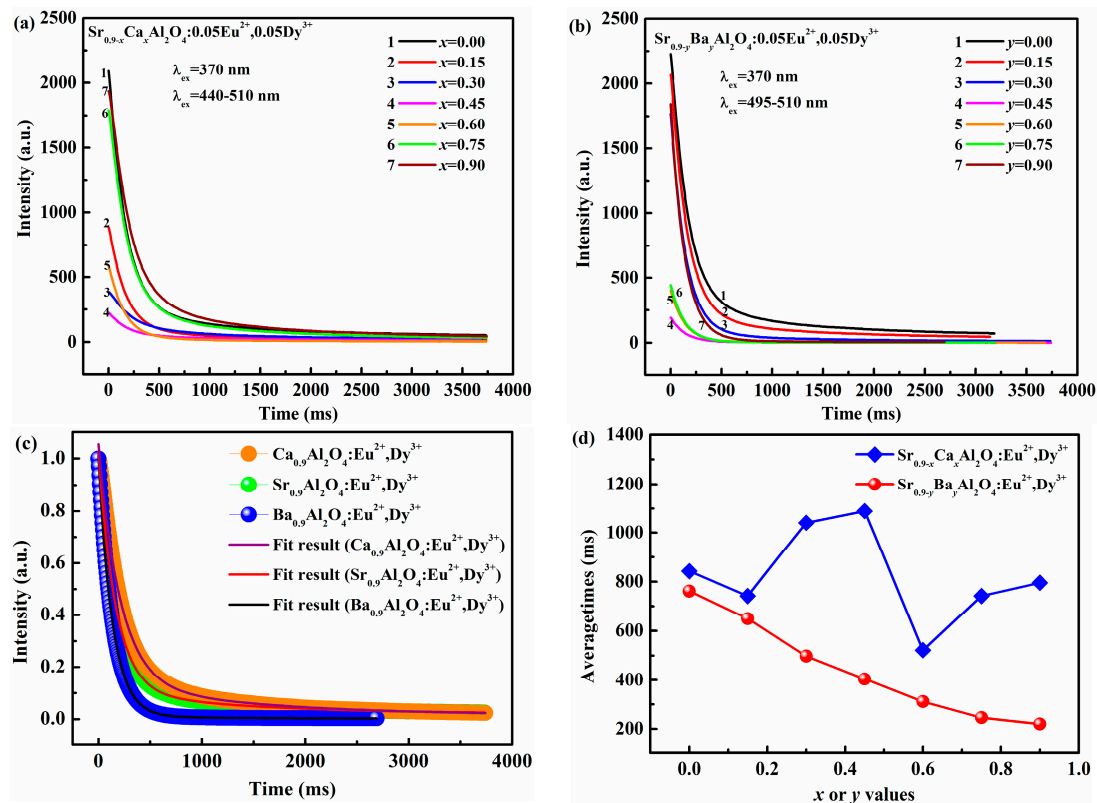

Figure 4. (**a**) Photoluminescence decay curves of $Sr_{0.90-x}Ca_xAl_2O_4:0.05Eu^{2+}$, $0.05Dy^{3+}$ with various $x(Ca^{2+})$ (λ_{ex} = 370 nm λ_{em} = 440–510 nm); (**b**) photoluminescence decay curves of $Sr_{0.90-y}Ba_yAl_2O_4:0.05Eu^{2+}$, $0.05Dy^{3+}$ with various $y(Ba^{2+})$ (λ_{ex} = 370 nm λ_{em} = 495–510 nm); (**c**) normalized decay and fitted curves of phosphors ($Ca_{0.90}Al_2O_4:0.05Eu^{2+}$, $0.05Dy^{3+}$, $Sr_{0.90}Al_2O_4:0.05Eu^{2+}$, $0.05Dy^{3+}$, $Ba_{0.90}Al_2O_4:0.05Eu^{2+}$, $0.05Dy^{3+}$); (**d**) average lifetimes of $Sr_{0.90-x}Ca_xAl_2O_4:0.05Eu^{2+}$, $0.05Dy^{3+}$, and $Sr_{0.90-y}Ba_yAl_2O_4:0.05Eu^{2+}$, $0.05Dy^{3+}$.

Moreover, the decay process of all samples is composed of fast decay, medium decay and subsequent of slow decay, which is consistent with our previous report. The decay curves of $Ca_{0.90}Al_2O_4:0.05Eu^{2+}$, $0.05Dy^{3+}$, $Sr_{0.90}Al_2O_4:0.05Eu^{2+}$, $0.05Dy^{3+}$, and $Ba_{0.90}Al_2O_4:0.05Eu^{2+}$, $0.05Dy^{3+}$ phosphors are fitted as representatives, which are presented in Figure 4c. The decay curves are well fitted with the following triple exponential functions:

$$I(t) = I_0 + Ae^{-t/\tau_1} + Be^{-t/\tau_2} + Ce^{-t/\tau_3} \tag{1}$$

where t is the time, I_0 and I is the luminescence intensity at initial time and t, respectively. A, B and C are constants. τ_1, τ_2, and τ_3 are the decay time for the exponential components, respectively. The average lifetimes can be obtained as follows. The detail parameters are listed in Table 2.

$$\tau_{average} = \frac{\int_0^\infty t \times I_{(\tau)} dt}{\int_0^\infty I_{(t)} dt} \tag{2}$$

Table 2. Results for fitted decay curve of $Ca_{0.90-x}Al_2O_4:0.05Eu^{2+}$, $0.05Dy^{3+}$, $Sr_{0.90-x}Al_2O_4:0.05Eu^{2+}$, $0.05Dy^{3+}$, and $Ba_{0.90-x}Al_2O_4:0.05Eu^{2+}$, $0.05Dy^{3+}$ phosphors.

Samples	Decay Lifetimes (ms)			
	τ_1	τ_2	τ_3	$\tau_{average}$
$Ca_{0.90}Al_2O_4:0.05Eu^{2+}$, $0.05Dy^{3+}$	210.28	210.28	1410.88	795.11
$Sr_{0.90}Al_2O_4:0.05Eu^{2+}$, $0.05Dy^{3+}$	1264.65	165.05	165.05	842.04
$Ba_{0.90}Al_2O_4:0.05Eu^{2+}$, $0.05Dy^{3+}$	134.50	1502.09	134.50	219.91

On the basis of the Equation (2), the average lifetime ($\tau_{average}$) of $SrAl_2O_4:Eu^{2+}$, Dy^{3+} phosphors with varied Ca^{2+} and Ba^{2+} contents are determined and shown in Figure 4d, respectively. The order of the average lifetimes is $Sr_{0.90}Al_2O_4:0.05Eu^{2+}$, $0.05Dy^{3+}$ > $Ca_{0.90}Al_2O_4:0.05Eu^{2+}$, $0.05Dy^{3+}$ > $Ba_{0.90}Al_2O_4:0.05Eu^{2+}$, $0.05Dy^{3+}$. The average lifetimes of $Sr_{0.90-x}Ca_xAl_2O_4:0.05Eu^{2+}$, $0.05Dy^{3+}$ phosphors vary with the change of Ca^{2+} content, and the maximum is about 1088.5 ms at $x = 0.45$. It could be ascribed to the complicate formation of the phase in Figure 1. Furthermore, the average lifetimes of $Sr_{0.90-y}Ba_yAl_2O_4:0.05Eu^{2+}$, $0.05Dy^{3+}$ phosphors gradually decrease with Ba^{2+} content increased due to the different phase formation and reach the shortest time of 219.91 ms at $y = 0.90$, demonstrating that the average lifetime or decay characteristics of $SrAl_2O_4:Eu^{2+}$, Dy^{3+} could be adjusted by the partial substitution of Ba^{2+}, Ca^{2+}. The results also indicate that the tuned lifetimes are more suitable for the application in AC-LEDs as the global widely utilize 50/60 Hz alternating current with a 5–20 ms dark duration.

3.4. Application of SrAl$_2$O$_4$:Eu^{2+}, Dy^{3+} Phosphors with Varied Contents of Ca^{2+} and Ba^{2+} in LEDs

Finally, phosphors converted LEDs were fabricated with silicone, near UV-chips (~365 nm, 395 nm), $Sr_{0.90-x}Ca_xAl_2O_4:0.05Eu^{2+}$, $0.05Dy^{3+}$, and $Sr_{0.90-y}Ba_yAl_2O_4:0.05Eu^{2+}$, $0.05Dy^{3+}$ phosphors. The phosphors account for 20% of the mass of silicone.

Figure 5 is the electroluminescence spectra of the as-fabricated LEDs based on $Sr_{0.90-x}Ca_xAl_2O_4:0.05Eu^{2+}$, $0.05Dy^{3+}$ phosphors and near UV Ga(In)N chips. In the Figure 4a, the shapes of all electroluminescence spectra in the as-fabricated LEDs are similar with the photoluminescence emission spectra of $Sr_{0.90-x}Ca_xAl_2O_4:0.05Eu^{2+}$, $0.05Dy^{3+}$ phosphors because the near UV around 365 nm of chips is completely absorbed by phosphors. Figure 5b depicts that the emission band located at 395 nm belongs to the UV-chips. And other emission bands are ascribed to Eu^{2+} emissions excited by 395 nm UV-chips. The results prove that the $Sr_{0.90-x}Ca_xAl_2O_4:0.05Eu^{2+}$, $0.05Dy^{3+}$ fluorescence materials can absorb the light with wavelength of 365 nm or 395 nm, and convert it into green or blue visible-light. The CIE color coordinates of as-fabricated LEDs are calculated and listed in Table 3. The inset of Figure 5 presents the chromaticity diagram of the as-fabricated LEDs based on $SrAl_2O_4:Eu^{2+}$, Dy^{3+} phosphors, which can be tuned from green to blue area and are similar with that of phosphors. In addition, the luminous efficiency is also systematically investigated under 20 mA forward-bias current in this work, as indicated in Figure 5c. The luminous efficiency of the as-fabricated LEDs with 395 nm is higher than in the case of 365 nm UV chips. However, for both kinds of LEDs fabricated by 365 nm and 395 nm UV-chips, the luminous efficiency decreases strongly, then increases slowly with Ca^{2+} content elevated. The maximum luminous efficiency is 11.24 lm/W for 365 nm LEDs and 35.35 lm/W for 395 nm LEDs ($x = 0$).
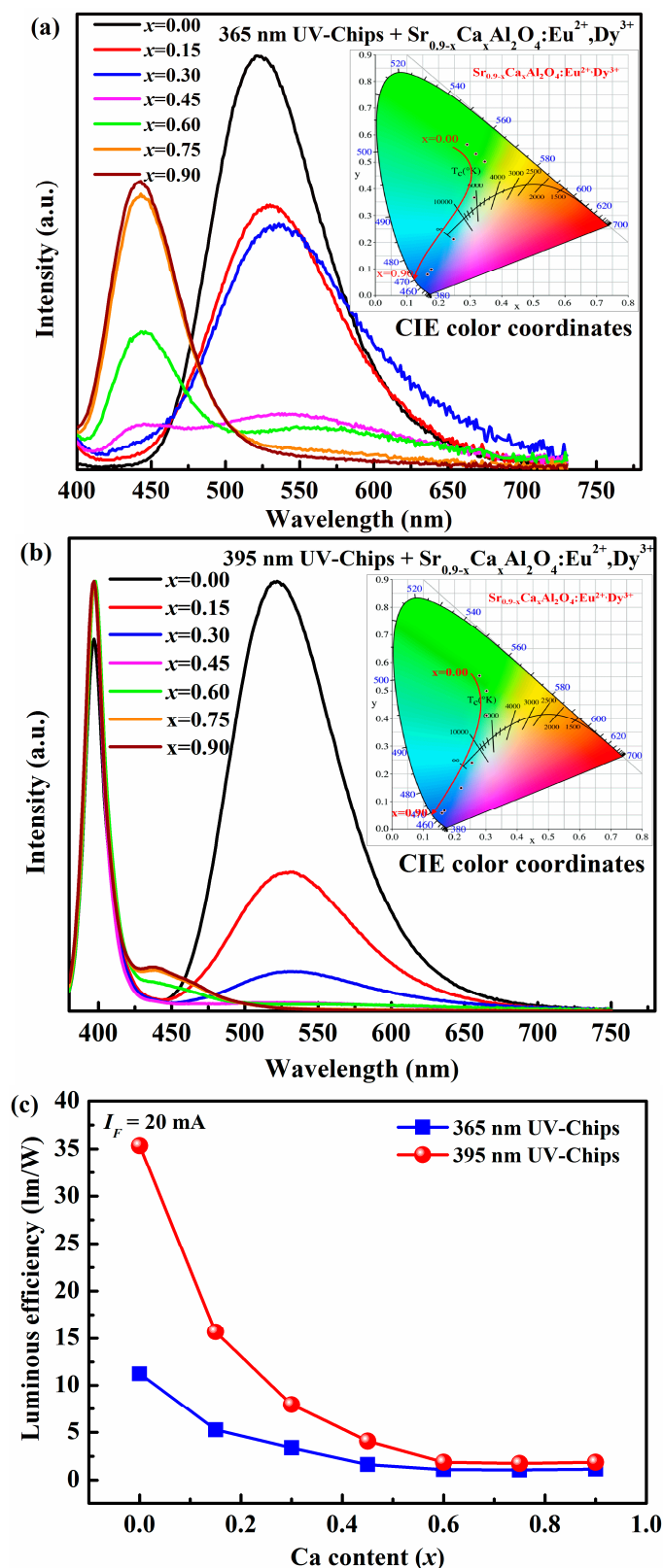
Figure 5. Electroluminescence spectra of the as-fabricated LEDs based on UV chip and $Sr_{0.90-x}Ca_xAl_2O_4$:0.05Eu^{2+}, 0.05Dy^{3+} phosphors under 20 mA forward-bias current (i.e., I_F = 20 mA). Inset is chromaticity diagram of the as-fabricated LEDs: (**a**) 365 nm UV chip; (**b**) 395 nm UV-chip; (**c**) Luminous efficiency of as-fabricated LEDs with different Ca^{2+} content under I_F = 20 mA.

Table 3. Parameter of chromaticity coordinates based on $Sr_{0.90-x}Ca_xAl_2O_4{:}0.05Eu^{2+}$, $0.05Dy^{3+}$ phosphors with 365 nm and 395 nm UV-Chips under 20 mA forward-bias current.

x Values	395 UV-Chips CIE (x, y)		365 UV-Chips CIE (x, y)	
	x	y	x	y
0.00	0.2805	0.5527	0.2907	0.5657
0.15	0.3029	0.5005	0.3181	0.5301
0.30	0.3033	0.4120	0.3462	0.5032
0.45	0.2555	0.2402	0.3139	0.3662
0.60	0.2209	0.1497	0.2486	0.2125
0.75	0.1675	0.0669	0.1771	0.0983
0.90	0.1599	0.0572	0.1655	0.0791

The electroluminescence spectra of LEDs based on $Sr_{0.90-x}Ba_xAl_2O_4{:}0.05Eu^{2+}$, $0.05Dy^{3+}$ phosphors are also investigated, as shown in Figure 6. Except emission peaks of the UV chip itself, all of the electroluminescence spectra of $Sr_{0.90-y}Ba_yAl_2O_4{:}0.05Eu^{2+}$, $0.05Dy^{3+}$ excited by both 365 nm and 395 nm UV-chips are similar. It indicates that the $Sr_{0.9-y}Ba_yAl_2O_4{:}Eu^{2+}$, Dy^{3+} phosphors can absorb 365 nm or 395 nm emission from Ga(N)In chips, and convert it into green or blue-green visible-light. The CIE color coordinates of the as-fabricated LEDs are calculated and listed in Table 4. By varying Ba^{2+} concentrations, the color of the as-fabricated LEDs can be tuned, but the adjustable zone is narrower than in the case of Ca^{2+}. It suggests that the color coordinates of pc-LEDs cannot be influenced by near UV Ga(In)N chips. However, the luminous efficiency decreases at first, and then increases with Ba^{2+} content enhanced. The maximum luminous efficiency is 11.26 lm/W for 365 nm LEDs and 33.34 lm/W for 395 nm LEDs ($y = 0$). The variation of luminous efficiency of the as-fabricated LED is also consistent with the emission spectra due to the different phase formation.
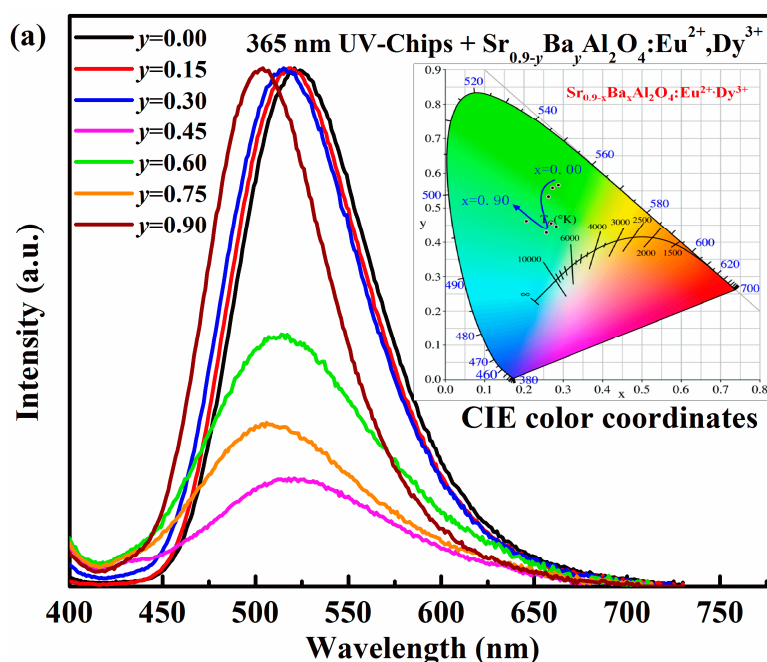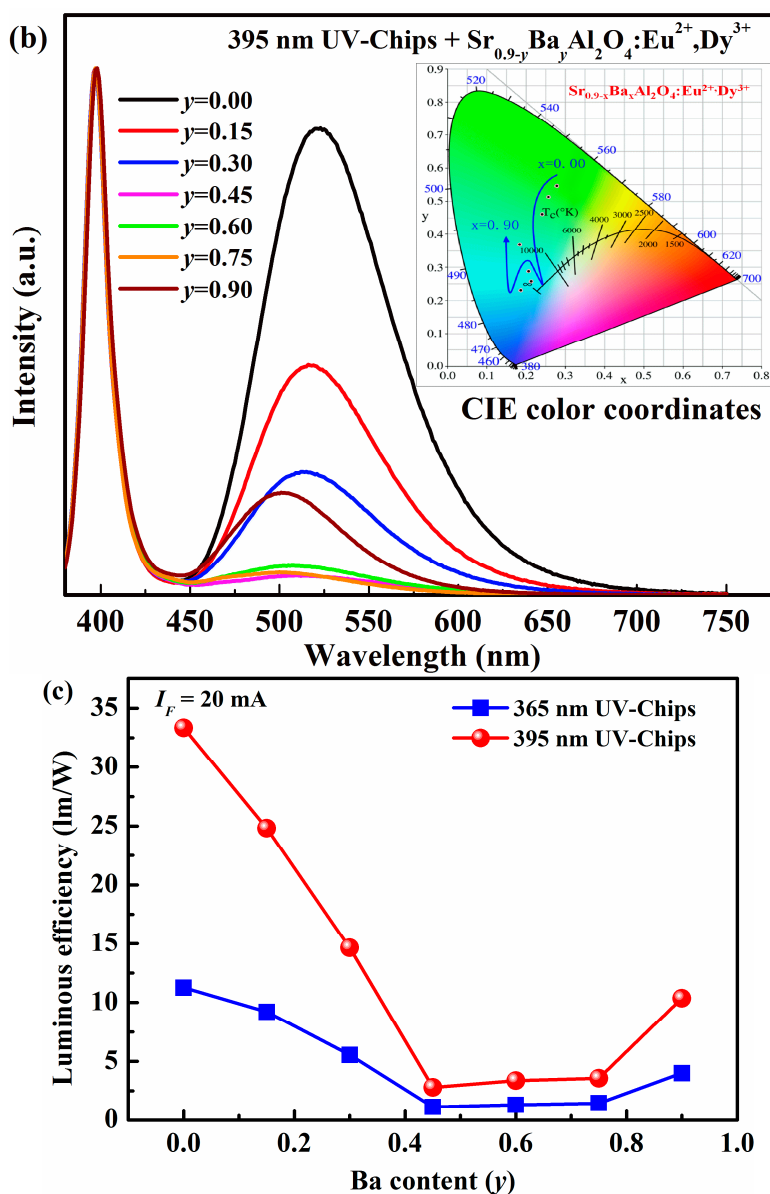

Figure 6. *Cont.*

Figure 6. Electroluminescence spectra of the as-fabricated LEDs based on UV-chip and $Sr_{0.90-y}Ba_yAl_2O_4$:0.05Eu^{2+}, 0.05Dy^{3+} phosphors under 20 mA forward-bias current (i.e., I_F = 20 mA). Inset is chromaticity diagram of the as-fabricated LEDs: (**a**) 365 nm UV-chip; (**b**) 395 nm UV-chip; (**c**) Luminous efficiency of as-fabricated LEDs with different Ba^{2+} content under I_F = 20 mA.

Table 4. Parameter of chromaticity coordinates based on $Sr_{0.90-x}Ba_xAl_2O_4$:0.05Eu^{2+}, 0.05Dy^{3+} phosphors with 365 nm and 395 nm UV-Chips under 20 mA forward-bias current.

y Values	395 UV-Chips		365 UV-Chips	
	CIE (x, y)		CIE (x, y)	
	x	y	x	y
0.00	0.2782	0.5471	0.2879	0.5666
0.15	0.2569	0.5045	0.2735	0.5584
0.30	0.2412	0.4612	0.2627	0.5331
0.45	0.2127	0.2568	0.2825	0.4471
0.60	0.2071	0.2881	0.2693	0.4560
0.75	0.1864	0.2309	0.2580	0.4278
0.90	0.1839	0.3678	0.2070	0.4628

4. Conclusions

$Sr_{0.90-x}Ca_xAl_2O_4$:0.05Eu^{2+}, 0.05Dy^{3+} and $Sr_{0.90-y}Ba_yAl_2O_4$:0.05Eu^{2+}, 0.05Dy^{3+} (x or y = 0.00, 0.15, 0.30, 0.45, 0.60, 0.75, 0.90) phosphors were synthesized. The variation of optical properties for the phosphors is ascribed to the phase structures. For the series of $Sr_{0.90-x}Ca_xAl_2O_4$:0.05Eu^{2+}, 0.05Dy^{3+} phosphors, two heterogeneous structures coexist, except the samples with $x(Ca^{2+})$ = 0.00 and 0.90. The emission color of $SrAl_2O_4$:Eu^{2+}, Dy^{3+} phosphor can be adjusted largely from green to blue, and the lifetime can also be tuned largely from 1088.5 ms to 521.6 ms. For $Sr_{0.90-y}Ba_yAl_2O_4$:0.05Eu^{2+}, 0.05Dy^{3+} phosphors, the phase transforms from monoclinic $SrAl_2O_4$ to hexagonal $BaAl_2O_4$ phase. Meanwhile, the emission wavelength shifts from 520 nm to 500 nm, and the color slightly changes from green to blue-green. More importantly, the average lifetime of $SrAl_2O_4$:Eu^{2+}, Dy^{3+} can be shortened from 842.04 ms to 219.91 ms, which can appropriately compensate for the AC time gap. Finally, the LEDs are successfully fabricated by combining the phosphors with Ga(In)N UV-chips. The maximum of luminous efficiency reaches 33.34 lm/W based on $SrAl_2O_4$:Eu^{2+}, Dy^{3+} phosphors.

Author Contributions: X.H. and M.Z. conceived and designed the experiments; Q.X. and B.L. performed the experiments; Y.C. and Q.Z. analyzed the data; M.Z. wrote the paper; X.H. revised the paper.

Conflicts of Interest: The authors declare no conflict of interest.

References

1. Suh, Y.; Kim, M.; Ahn, C.-H. Novel flicker migration and EMI noise reduction circuit for AC direct LED lightings. *J. Electr. Eng. Technol.* **2017**, *12*, 874–879. [CrossRef]

2. Yeh, C.-W.; Li, Y.; Wang, J.; Liu, R.-S. Appropriate green phosphor of $SrSi_2O_2N_2$:Eu^{2+}, Mn^{2+} for AC LEDs. *Opt. Express* **2012**, *20*, 18031–18043. [CrossRef] [PubMed]

3. Lin, H.; Wang, B.; Xu, J.; Zhang, R.; Chen, H.; Yu, Y.; Wang, Y. Phosphor-in-glass for high-powered remote-type white AC-LED. *ACS Appl. Mater. Interfaces* **2014**, *6*, 21264–21269. [CrossRef] [PubMed]

4. Li, B.; Zhang, J.; Zhang, M.; Long, Y.; He, X. Effects of $SrCl_2$ as a flux on the structural and luminescent properties of $SrAl_2O_4$:Eu^{2+}, Dy^{3+} phosphors for AC-LEDs. *J. Alloys Compd.* **2015**, *651*, 497–502. [CrossRef]

5. Chen, L.; Zhang, Y.; Liu, F.; Luo, A.; Chen, Z.; Jiang, Y.; Chen, S.; Liu, R.-S. A new green phosphor of $SrAl_2O_4$:Eu^{2+}, Ce^{3+}, Li^+ for alternating current driven light-emitting diodes. *Mater. Res. Bull.* **2012**, *47*, 4071–4075. [CrossRef]

6. Tan, J.; Narendran, N. Defining phosphor luminescence property requirements for white AC LED flicker reduction. *J. Lumin.* **2015**, *167*, 21–26. [CrossRef]

7. Chen, L.; Zhang, Y.; Xue, S.; Deng, X.; Luo, A.; Liu, F.; Jiang, Y.; Chen, S.; Bahader, A. The green phosphor $SrAl_2O_4$:Eu^{2+}, R^{3+} (R = Y, Dy) and its application in alternating current light-emitting diodes. *Funct. Mater. Lett.* **2013**, *6*. [CrossRef]

8. Rojas-Hernandez, R.E.; Rubio-Marcos, F.; Enríquez, E.; De La Rubia, M.A.; Fernandez, J.F. A low-energy milling approach to reduce particle size maintains the luminescence of strontium aluminates. *RSC Adv.* **2015**, *5*, 42559–42567. [CrossRef]

9. Nagamani, S.; Panigrahi, B.S. Luminescence properties of SrO-Al_2O_3:Eu^{2+}, Dy^{3+} prepared at different temperatures. *J. Am. Ceram. Soc.* **2010**, *93*, 3832–3836. [CrossRef]

10. Rahimi, M.R.; Yun, G.J.; Doll, G.L.; Choi, J.S. Effects of persistent luminescence decay on mechanoluminescence phenomena of $SrAl_2O_4$:Eu^{2+}, Dy^{3+} materials. *Opt. Lett.* **2013**, *38*, 4134–4137. [CrossRef] [PubMed]

11. Timilsina, S.; Lee, K.H.; Kwon, Y.N.; Kim, J.S.; Reimanis, I. Optical evaluation of in situ crack propagation by using mechanoluminescence of $SrAl_2O_4$:Eu^{2+}, Dy^{3+}. *J. Am. Ceram. Soc.* **2015**, *98*, 2197–2204. [CrossRef]

12. Katsumata, T.; Toyomane, S.; Sakai, R.; Komuro, S.; Morikawa, T. Trap levels in Eu-doped $SrAl_2O_4$ phosphor crystals co-doped with rare-earth elements. *J. Am. Ceram. Soc.* **2006**, *89*, 932–936. [CrossRef]

13. Liu, C.; Wang, Y.; Hu, Y.; Chen, R.; Liao, F. Adjusting luminescence properties of $Sr_xCa_{1-x}Al_2O_4$:Eu^{2+}, Dy^{3+} phosphors by Sr/Ca ratio. *J. Alloy. Compd.* **2009**, *470*, 473–476. [CrossRef]

14. Xie, W.; Quan, J.; Wu, H.; Shao, L.; Zou, C.; Zhang, J.; Shi, X.; Wang, Y. Structure and luminescence properties of $SrAl_2O_4$:Eu^{2+}, Dy^{3+} by Ba^{2+} and Ca^{2+} co-doping. *J. Alloys Compd.* **2012**, *514*, 97–102. [CrossRef]

15. Das, S.; Yang, C.-Y.; Lin, H.-C.; Lu, C.-H. Structural and luminescence properties of tunable white-emitting $Sr_{0.5}Ca_{0.5}Al_2O_4$:Eu^{2+}, Dy^{3+} for UV-excited white-LEDs. *RSC Adv.* **2014**, *4*, 64956–64966. [CrossRef]

16. Shi, W.S.; Yamada, H.; Nishikubo, K.; Kusaba, H.; Xu, C.N. Novel structural behavior of strontium aluminate doped with europium. *J. Electrochem. Soc.* **2004**, *151*, H97–H100. [CrossRef]

17. Ju, S.H.; Kim, S.G.; Choi, J.C.; Park, H.L.; Mho, S.I.; Kim, T.W. Determination of the solid solubility of $SrAl_2O_4$ in $CaAl_2O_4$ through crystal field-dependent Eu^{2+} signatures. *Mater. Res. Bull.* **1999**, *34*, 1905–1909. [CrossRef]

18. Pololla, F.C.; Levine, A.K.; Tomkus, M.R. Fluorescent properties of alkaline earth aluminates of the type MAl_2O_4 activated by divalent europium. *J. Electrochem. Soc.* **1968**, *115*, 642–644. [CrossRef]

19. Nazarov, M.; Brik, M.G.; Spassky, D.; Tsukerblat, B. Crystal field splitting of 5d states and luminescence mechanism in $SrAl_2O_4$:Eu^{2+} phosphor. *J. Lumin.* **2017**, *182*, 79–86. [CrossRef]

20. Bachmann, V.; Ronda, C.; Oeckler, O.; Schnick, W.; Meijerink, A. Color point tuning for (Sr, Ca, Ba)$Si_2O_2N_2$:Eu^{2+} for white light LEDs. *Chem. Mater.* **2009**, *21*, 316–325. [CrossRef]

21. Ye, S.; Xiao, F.; Pan, Y.X.; Ma, Y.Y.; Zhang, Q.Y. Phosphors in phosphor-converted white light-emitting diodes: Recent advances in materials, techniques and properties. *Mater. Sci. Eng. R Rep.* **2010**, *71*, 1–34. [CrossRef]

22. Sommer, C.; Hartmann, P.; Pachler, P.; Hoschopf, H.; Wenzl, F.P. The phosphor's optical properties—Chromaticity coordinate relationship of phosphor converted white LEDs. *Opt. Quantum Electron.* **2011**, *44*, 111–117. [CrossRef]